Available online at www.sciencedirect.com
ScienceDirect
Chinese Journal of Aeronautics 20(2007) 425-433

Chinese Journal of Aeronautics
www.elsevier.com/locate/cja

Adaptive Sliding Control of Six-DOF Flight Simulator Motion Platform

Wu Dongsu*, Gu Hongbin

College of Civil Aviation, Nanjing University of Aeronautics and Astronautics, Nanjing 210016, China

Received 29 September 2006; accepted 28 April 2007

Abstract

There is proposed an adaptive sliding controller in task space on the base of the linear Newton-Euler dynamic equation of motion platform in a six-DOF flight simulator. The uncertain parameters are divided into two groups: the constant and the time-varying. The controller identifies constant uncertain parameters using nonlinear adaptive controller associated with elimination of the influences of time-varying uncertain parameters and compensation of the external disturbance using sliding control. The results of numerical simulation attest to the capability of this control scheme not only to, with deadly accuracy, identify parameters of motion platform such as load, inertia moments and mass center, but also effectively improve the robustness of the system.

Keywords: motion platform; nonlinear adaptive control; sliding control; flight simulator; Stewart platform

1 Introduction

The development of flight simulators bears close relation to the advance of modern aircraft. A flight simulator has two most important functions, one is flight training, the other is research and development[1]. In flight training, it is used mainly to reduce cost and increase safety, while in research and development, it performs flight simulation to evaluate the controllability of a new airplane or the performances of a newly devised component prior to its flight testing. Another kind of flight simulator is used to determine the causal factors in an accident and replicate the accident scenario[2]. In order to fulfill the above-mentioned functions, flight simulation must imitate flight and provide realistic information that indicates a vehicle motion in three ways: ① from visual system with naked eyes; ② from vestibular system; ③ from tactile system, in which, for instance, the acceleration of a vehicle is perceived from the force that the seat exerts on a pilot's back.

As an important element of a flight simulator, the motion platform serves to simulate the motion of aircraft and provides the pilot with realistic vestibular feelings and a part of tactile feelings. According to the FAA regulations, any device called "flight simulator" must have at least one motion platform, otherwise it can only be termed a "flight training device". A motion platform in flight simulator is often constituted of parallel mechanisms due to the requirements of bearing heavy loads and performing flexible movements. Among parallel platforms, six-DOF Stewart platforms[3] gain most popularity in medium- and light-load situations. But a Stewart platform, due to its inclusion of several close-loop structures, is more complicated to make kinematics analysis, dynamics analysis and control than a conventional serial mechanism.

Pending the span of last two decades, re-

*Corresponding author. Tel.: +86-25-84890755.
E-mail address: tissle@nuaa.edu.cn

searches of Stewart platforms focused on the realm of kinematics inclusive of inverse and direct kinematics solutions[4], workspace analysis and singularity analysis. In contrast to the large amount of published literature on the kinematics analysis of Stewart platform, fewer results have been made in public on its dynamics and control[5]. Currently one of the main methods of modeling dynamics of Stewart platform, the Lagrange equation[6], well structured and clearly expressed notwithstanding, demands a vast amount of symbolic calculation to find partial derivatives of the Lagrangian thus leading to being unfit for real-time computation. The Newton-Euler equation[7], in spite of its simple concept and ease to derive, requires computation of all constraint forces. There are other methods including principle of virtual work, Kane equation, etc. The control strategies for a parallel mechanism can be roughly split into two schemes: joint space control and task space control. The joint space control scheme uses inverse kinematics to compute the target position of every actuator from the target position of platform followed by an application of the independent close-loop PD control to every actuator. This control scheme is adopted by most motion controllers in conventional flight simulators because of their convenience to operate. However, serious degradation of performances often happens due to cross coupling of parallel mechanisms when they move with large amplitudes and high velocity. Other factors such as manufacturing errors, friction forces, load changes and external disturbance also bring negative influences to bear on the performances of a conventional PD controller. To solve this problem, Su et al.[8] proposed a nonlinear PD controller with velocity estimation on joint space to offset nonlinearity, disturbance and friction. Some other novel joint space controllers use a dynamic model of platform to make up for the nonlinearity. Honegger et al.[9] came up with a simplified linearly parameterized dynamic model of a Hexslide parallel mechanism using tracking errors to adaptively identify uncertain parameters and improving gradually tracking performances. Nevertheless, the simplification of actuators in the dynamic model also produces negative effects on control performances in some cases. Kang et al.[10] put forward a robust nonlinear controller for a parallel system driven by a hydraulic-servo system based on the Lyapunov redesign method, but the uncertainties chosen in it are too conservative. The task space control scheme is another kind of control strategy. Although it needs direct measurement or estimation of platform's status data, better performances than joint space controller can be achieved because of its direct use of target position and involvement of concerns about uncertainty and disturbance in the controller design process. Ting et al.[11] introduced a composite adaptive controller in task space ensuring converge of tracking errors and parameter estimation based on Lyapunov method. But this model fails to take external disturbance into account. A robust nonlinear controller developed by Kim et al.[12] is equipped with a friction estimator in task space and experimentally its control performances are almost comparable to joint space PD controller and task space nonlinear controller. However, little attention is paid to parameter changes like the payload change in designing.

A complete linear dynamic model of motion platform in flight simulator using Newton-Euler method is suggested and a nonlinear adaptive sliding controller in task space based on a model capable of achieving precise motion control in the presence of uncertain parameters as well as external disturbances is proposed. In this control scheme, uncertain parameters are divided into two parts: ① constant uncertain parameters such as loads, inertial moments, and mass center, etc. ② time-varying uncertain parameters and external disturbances such as friction forces, torque fluctuation of motor, etc. A nonlinear self-adaptive control is adopted to identify the constant uncertain parameters on-line while a sliding control to tackle time-varying uncertain parameters as well as external disturbances. Finally, simulation of the closed-loop system incorporated with the nonlinear adaptive sliding controller is carried out to demonstrate the effectiveness of parameter identification and disturbance rejection.

2 Model of Motion Platform in Flight Simulator

A motion platform in a six-DOF flight simulator is of an electrical driven ball screw type 6-3 UPS Stewart platform. After a brief analysis of the inverse kinematics and direct kinematics of a platform, a dynamic model of the platform is derived by means of Newton-Euler method. Then the model is simplified into a linear form with a combination of uncertain parameters used in nonlinear self-adaptive control and sliding control. Fig.1 demonstrates the structure of a Stewart platform.

2.1 Kinematics analysis of a motion platform

(1) Inverse kinematics analysis

Inverse kinematics of a Stewart platform can transform the movement of a moving platform related to fix platform into the movement of each actuator. Let $\{\boldsymbol{B}\}$ and $\{\boldsymbol{P}\}$ be the coordinates of the base platform and the payload platform correspondingly, and suppose that vector $\boldsymbol{P}_i = [P_{ix} \ \ P_{iy} \ \ P_{iz}]^{\mathrm{T}}$ describes the position of the reference point connecting ith actuator and payoad platform in $\{\boldsymbol{P}\}$, vector $\boldsymbol{B}_i = [b_{ix} \ \ b_{iy} \ \ b_{iz}]^{\mathrm{T}}$ describes the position of the reference point connecting ith actuator and base platform in $\{\boldsymbol{B}\}$, and rotation matrix $\boldsymbol{R}$ represents the orientation of the frame $\{\boldsymbol{P}\}$ with respect to the frame $\{\boldsymbol{B}\}$, then

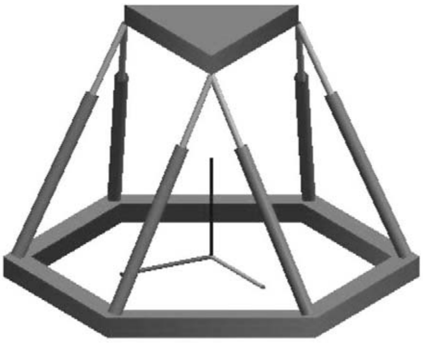

Fig.1 Structure of a Stewart platform.

$$\boldsymbol{R}=\begin{bmatrix} R_{11} & R_{12} & R_{13} \\ R_{21} & R_{22} & R_{23} \\ R_{31} & R_{32} & R_{33} \end{bmatrix}=\begin{bmatrix} \cos\alpha\times\cos\beta & \cos\alpha\times\sin\beta\times\sin\gamma-\sin\alpha\times\cos\gamma & \cos\alpha\times\sin\beta\times\cos\gamma+\sin\alpha\times\sin\gamma \\ \sin\alpha\times\cos\beta & \sin\alpha\times\sin\beta\times\sin\gamma+\cos\alpha\times\cos\gamma & \sin\alpha\times\sin\beta\times\cos\gamma-\cos\alpha\times\sin\gamma \\ -\sin\beta & \cos\beta\times\sin\gamma & \cos\beta\times\cos\gamma \end{bmatrix} \tag{1}$$

By proper coordinate transformation, the ith actuator vector $\boldsymbol{L}_i$ can be written as

$$\boldsymbol{L}_i=\boldsymbol{R}\cdot\boldsymbol{P}_i+\boldsymbol{T}-\boldsymbol{B}_i,\ i=1,2,\cdots,6 \tag{2}$$

where $\boldsymbol{T}=[t_x \ t_y \ t_z]^{\mathrm{T}}$ represents the vector from the origin of payload platform to the origin of base platform. $l_i=\|\boldsymbol{L}_i\|$ is the length of the ith actuator.

(2) Direct kinematics analysis

Direct kinematics is the inverse problem of inverse kinematics, which entails computation of the six-DOF information of payload platform from the given lengths of six actuators. Direct kinematics of Stewart platform plays an important role in the task space control because it can estimate the motion information of the payload platform on-line in place of using expensive sensors. Expressed as a 16-order polynomial, the analytical solutions of direct kinematics can not be solved real-time leading to the necessity of using the Newton-Raphson method to acquire the numerical solution[13].The computational result of a target position will not be singular as long as the initial position is not singular. To speed up converge of the Newton-Raphson method, the initial position might well be defined as the last target position.

2.2 Dynamic model of motion platform in Newton-Euler equation

The dynamic equation of a Stewart platform expressed in the Newton-Euler equation is

$$\boldsymbol{M}(\boldsymbol{X})\ddot{\boldsymbol{X}}+\boldsymbol{H}(\boldsymbol{X},\dot{\boldsymbol{X}})=\boldsymbol{J}^{\mathrm{T}}\boldsymbol{F}+\boldsymbol{D} \tag{3}$$

where $\boldsymbol{X},\dot{\boldsymbol{X}},\ddot{\boldsymbol{X}}$ separately correspond to position, velocity and acceleration information of a payload platform in task space, $\boldsymbol{M}(\boldsymbol{X})$ is the inertia matrix, $\boldsymbol{H}(\boldsymbol{X},\dot{\boldsymbol{X}})$ the nonlinearity including Coriolis, centrifugal and gravity force, $\boldsymbol{F}$ the driving force of actuators, $\boldsymbol{J}$ the Jacobian matrix and $\boldsymbol{D}$ the external disturbance.

The individual constituents of this equation can be expressed as follows:

$$\boldsymbol{M}(\boldsymbol{X}) = \boldsymbol{M}_{\mathrm{p}} + \sum_{i=1}^{6} \boldsymbol{M}_i$$

$$\boldsymbol{H}(\boldsymbol{X}, \dot{\boldsymbol{X}}) = \boldsymbol{H}_{\mathrm{p}} + \sum_{i=1}^{6} \boldsymbol{H}_i$$

$$\boldsymbol{M}_{\mathrm{p}} = \begin{bmatrix} m\boldsymbol{E}_3 & -m\tilde{\boldsymbol{r}} \\ m\tilde{\boldsymbol{r}} & \boldsymbol{I} + m\,(|\boldsymbol{r}|^2\ \boldsymbol{E}_3 - \boldsymbol{r}\boldsymbol{r}^{\mathrm{T}}) \end{bmatrix}$$

$$\boldsymbol{M}_i = \begin{bmatrix} \boldsymbol{Q}_i & -\boldsymbol{Q}_i\tilde{\boldsymbol{q}}_i \\ \tilde{\boldsymbol{q}}_i\boldsymbol{Q}_i & -\tilde{\boldsymbol{q}}_i\boldsymbol{Q}_i\tilde{\boldsymbol{q}}_i \end{bmatrix}$$

$$\boldsymbol{H}_{\mathrm{p}} = \begin{bmatrix} m\,[\boldsymbol{\omega}\times(\boldsymbol{\omega}\times\boldsymbol{r}) - \boldsymbol{g}] \\ \boldsymbol{\omega}\times\boldsymbol{I}\boldsymbol{\omega} + m\boldsymbol{r}\times[(\boldsymbol{\omega}\cdot\boldsymbol{r})\boldsymbol{\omega} - \boldsymbol{g}] \end{bmatrix}$$

$$\boldsymbol{H}_i = \begin{bmatrix} \boldsymbol{V}_i \\ \boldsymbol{q}_i \times \boldsymbol{V}_i - \boldsymbol{f}_i \end{bmatrix}$$

$$J = \begin{bmatrix} \boldsymbol{u}_1 & \boldsymbol{u}_2 & \boldsymbol{u}_3 & \boldsymbol{u}_4 & \boldsymbol{u}_5 & \boldsymbol{u}_6 \\ \boldsymbol{q}_1\times\boldsymbol{u}_1 & \boldsymbol{q}_2\times\boldsymbol{u}_2 & \boldsymbol{q}_3\times\boldsymbol{u}_3 & \boldsymbol{q}_4\times\boldsymbol{u}_4 & \boldsymbol{q}_5\times\boldsymbol{u}_5 & \boldsymbol{q}_6\times\boldsymbol{u}_6 \end{bmatrix}$$

$$\boldsymbol{q}_i = \boldsymbol{R}\boldsymbol{P}_i$$

$$\boldsymbol{r} = \boldsymbol{R}\boldsymbol{r}_{\mathrm{p}}$$

$$\boldsymbol{I} = \boldsymbol{R}\boldsymbol{I}_{\mathrm{p}}\boldsymbol{R}^{\mathrm{T}}$$

$$\boldsymbol{V}_i = \boldsymbol{U}_i + \boldsymbol{f}_{\mathrm{b}i}\ \mathrm{sgn}(\dot{\boldsymbol{L}}_i)$$

where $\boldsymbol{M}_{\mathrm{p}}$ is the inertia matrix of a payload platform, $\boldsymbol{M}_i$ the inertia matrix of the ith actuator, $\boldsymbol{H}_{\mathrm{p}}$ the nonlinearity term of the payload platform, $\boldsymbol{H}_i$ the nonlinearity term of the ith actuator, m the mass of the payload platform, $\boldsymbol{\omega} = [\omega_x \quad \omega_y \quad \omega_z]^{\mathrm{T}}$ the angular velocity of the payload platform in task space, $\boldsymbol{u}_i$ the unit vector of the ith actuator, $\boldsymbol{f}_i$ the Coulomb and viscous friction forces on the link point of the ith actuator and the payload platform, $\boldsymbol{r}_{\mathrm{p}}$ the center of gravity of the payload platform, $\boldsymbol{I}_{\mathrm{p}}$ the inertia moment of the payload platform, $\boldsymbol{E}_3$ the 3×3 identity matrix, $\boldsymbol{g} = [0 \quad 0 \quad g]^{\mathrm{T}}$ the gravity acceleration vector, $\boldsymbol{q}_i$, $\boldsymbol{r}$ and $\boldsymbol{I}$ the transformation of $\boldsymbol{P}_i$, $\boldsymbol{r}_{\mathrm{p}}$ and $\boldsymbol{I}_{\mathrm{p}}$ from the payload platform reference frame to global basis, $\boldsymbol{f}_{\mathrm{b}i}$ the Coulomb and viscous friction force between ball screws and nut caps, $\mathrm{sgn}(\dot{\boldsymbol{L}}_i)$ the moving direction of the ith actuator, $\boldsymbol{Q}_i$ and $\boldsymbol{V}_i$ related to the ith actuator, the specific form of which can be found in Ref.[7], $\boldsymbol{U}_i$ the remaining part of $\boldsymbol{V}_i$ from which the friction forces has been deducted, $\tilde{\boldsymbol{q}}_i$ and $\tilde{\boldsymbol{r}}$ the transformation of $\boldsymbol{q}_i$ and $\boldsymbol{r}$ from cross product to normal matrix multiplication.

2.3 Linear form of dynamic model

The application of nonlinear self-adaptive control and sliding control requires the dynamic model of the motion platform to be transformed into a linear form

$$\boldsymbol{M}(\boldsymbol{X})\ddot{\boldsymbol{X}} + \boldsymbol{H}(\boldsymbol{X}, \dot{\boldsymbol{X}}) = \boldsymbol{Y}\boldsymbol{p}$$

where $\boldsymbol{p}$ is a vector containing uncertain parameters.

The uncertain parameters of the motion platform of six-DOF flight simulator consist of two parts: one is due to the differences of payloads of, for instance, trainees and devices, which include mass, inertia moments and center of gravity of the payload platform; the other is caused by friction forces. Since the mass of the payload platform is located on the center of the x and y axis, the center of gravity can be simplified as $\boldsymbol{r}_{\mathrm{p}} = [0 \quad 0 \quad r_z]^{\mathrm{T}}$, and the inertia moment is denoted by $\boldsymbol{I}_{\mathrm{p}} = \mathrm{diag}\,(I_{xx} \quad I_{yy} \quad I_{zz})$. Meanwhile, with the friction forces on the link points of actuators and platform omitted, the only considered friction forces are the ones between ball screws and nut caps. Consequently, $\boldsymbol{p}$ and $\boldsymbol{Y}$ can be expressed as follows:

$$\begin{aligned} \boldsymbol{p} = [&m \ \ I_{xx} \ \ I_{yy} \ \ I_{zz} \ \ mr_z \ \ mr_z^2 \\ &f_{\mathrm{b}1} \ \ f_{\mathrm{b}2} \ \ f_{\mathrm{b}3} \ \ f_{\mathrm{b}4} \ \ f_{\mathrm{b}5} \ \ f_{\mathrm{b}6} \ \ 1]^{\mathrm{T}} \end{aligned} \tag{4}$$

$$\begin{aligned} \boldsymbol{Y} = [&\boldsymbol{Y}_1 \ \ \boldsymbol{Y}_2 \ \ \boldsymbol{Y}_3 \ \ \boldsymbol{Y}_4 \ \ \boldsymbol{Y}_5 \ \ \boldsymbol{Y}_6 \ \ \boldsymbol{Y}_{71} \\ &\boldsymbol{Y}_{72} \ \ \boldsymbol{Y}_{73} \ \ \boldsymbol{Y}_{74} \ \ \boldsymbol{Y}_{75} \ \ \boldsymbol{Y}_{76} \ \ \boldsymbol{Y}_8] \end{aligned} \tag{5}$$

where

$$\boldsymbol{Y}_1 = \begin{bmatrix} \boldsymbol{E}_3 & \boldsymbol{0} \\ \boldsymbol{0} & \boldsymbol{0} \end{bmatrix}\ddot{\boldsymbol{X}} + \begin{bmatrix} -\boldsymbol{g} \\ \boldsymbol{0} \end{bmatrix}$$

$$\ddot{\boldsymbol{X}} = \begin{bmatrix} \ddot{X}_1 & \ddot{X}_2 & \ddot{X}_3 & \ddot{X}_4 & \ddot{X}_5 & \ddot{X}_6 \end{bmatrix}^{\mathrm{T}}$$

$$\boldsymbol{Y}_2 = \begin{bmatrix} 0 & 0 & 0 & Y_{21} & Y_{22} & Y_{23} \end{bmatrix}^{\mathrm{T}}$$

$$\begin{aligned} Y_{2i} = {} & R_{1i}^2\ddot{X}_4 + R_{1i}R_{2i}\ddot{X}_5 + R_{1i}R_{3i}\ddot{X}_6 + \omega_y(R_{1i}R_{3i}\omega_x + \\ & R_{2i}R_{3i}\omega_y + R_{3i}^2\omega_z) - \omega_z(R_{1i}R_{2i}\omega_x + \\ & R_{2i}^2\omega_y + R_{2i}R_{3i}\omega_z), \quad i = 1,2,3 \end{aligned}$$

$$\boldsymbol{Y}_3 = \begin{bmatrix} 0 & 0 & 0 & Y_{31} & Y_{32} & Y_{33} \end{bmatrix}^{\mathrm{T}}$$

$$\begin{aligned} Y_{3i} = {} & R_{1i}R_{2i}\ddot{X}_4 + R_{2i}^2\ddot{X}_5 + R_{2i}R_{3i}\ddot{X}_6 + \omega_z(R_{1i}^2\omega_x + \\ & R_{1i}R_{2i}\omega_y + R_{1i}R_{3i}\omega_z) - \omega_x(R_{1i}R_{3i}\omega_x + \\ & R_{2i}R_{3i}\omega_y + R_{3i}^2\omega_z), \quad i = 1,2,3 \end{aligned}$$

$$\boldsymbol{Y}_4=\begin{bmatrix}0 & 0 & 0 & Y_{41} & Y_{42} & Y_{43}\end{bmatrix}^{\mathrm{T}}$$

$$Y_{4i}=R_{1i}R_{3i}\ddot{X}_4+R_{2i}R_{3i}\ddot{X}_5+R_{3i}^2\ddot{X}_6+\omega_x(R_{1i}R_{2i}\omega_x+R_{2i}^2\omega_y+R_{2i}R_{3i}\omega_z)-\omega_y(R_{1i}^2\omega_x+R_{1i}R_{2i}\omega_y+R_{1i}R_{3i}\omega_z),\quad i=1,2,3$$

$$\boldsymbol{Y}_5=\begin{bmatrix}\boldsymbol{0} & -\boldsymbol{Y}_{50}\\ \boldsymbol{Y}_{50} & \boldsymbol{0}\end{bmatrix}\ddot{\boldsymbol{X}}+\begin{bmatrix}\boldsymbol{Y}_{51} & \boldsymbol{0}\end{bmatrix}^{\mathrm{T}}$$

$$\boldsymbol{Y}_{50}=\begin{bmatrix}0 & -R_{33} & R_{23}\\ R_{33} & 0 & -R_{13}\\ -R_{23} & R_{13} & 0\end{bmatrix}$$

$$\boldsymbol{Y}_{51}=\begin{bmatrix}\omega_x\omega_yR_{23}+\omega_x\omega_zR_{33}-\omega_y^2R_{13}-\omega_z^2R_{13}\\ \omega_x\omega_yR_{13}+\omega_y\omega_zR_{33}-\omega_x^2R_{23}-\omega_z^2R_{23}\\ \omega_x\omega_zR_{13}+\omega_y\omega_zR_{23}-\omega_x^2R_{33}-\omega_y^2R_{33}\\ gR_{23}\\ -gR_{13}\end{bmatrix}^{\mathrm{T}}$$

$$\boldsymbol{Y}_6=\begin{bmatrix}\boldsymbol{0} & \boldsymbol{0}\\ \boldsymbol{0} & \boldsymbol{Y}_{60}\end{bmatrix}\ddot{\boldsymbol{X}}+\begin{bmatrix}0 & 0 & 0 & \boldsymbol{Y}_{61}\end{bmatrix}^{\mathrm{T}}$$

$$\boldsymbol{Y}_{60}=\begin{bmatrix}0 & -R_{13}R_{23} & -R_{13}R_{33}\\ -R_{13}R_{23} & 0 & -R_{23}R_{33}\\ -R_{13}R_{33} & -R_{23}R_{33} & 0\end{bmatrix}$$

$$\boldsymbol{Y}_{61}=\begin{bmatrix}(R_{23}\omega_z-R_{33}\omega_y)(R_{13}\omega_x+R_{23}\omega_y+R_{33}\omega_z)\\ (R_{33}\omega_x-R_{13}\omega_z)(R_{13}\omega_x+R_{23}\omega_y+R_{33}\omega_z)\\ (R_{13}\omega_y-R_{23}\omega_x)(R_{13}\omega_x+R_{23}\omega_y+R_{33}\omega_z)\end{bmatrix}^{\mathrm{T}}$$

$$\boldsymbol{Y}_{7i}=\begin{bmatrix}\boldsymbol{u}_i & \boldsymbol{q}_i\times\boldsymbol{u}_i\end{bmatrix}^{\mathrm{T}}\operatorname{sgn}(\dot{\boldsymbol{L}}_i),\quad i=1,2,\cdots,6$$

$$\boldsymbol{Y}_8=\sum_{i=1}^{6}\boldsymbol{M}_i\cdot\ddot{\boldsymbol{X}}+\sum_{i=1}^{6}\begin{bmatrix}\boldsymbol{U}_i\\ \boldsymbol{q}_i\times\boldsymbol{U}_i\end{bmatrix}$$

The above equations can be formulated as

$$\boldsymbol{Yp}=\boldsymbol{J}^{\mathrm{T}}\boldsymbol{F}+\boldsymbol{D}$$

therefore, the dynamic model of a motion platform takes on a linear form. The vector $\boldsymbol{p}$ can further be divided into three parts. The first is the constant uncertain parameter—something that changes very slowly or does not change at all when the whole system is running. In this case, $\boldsymbol{p}_{\mathrm{a}}=[m\quad I_{xx}\quad I_{yy}\quad I_{zz}\quad mr_z\quad mr_z^2]^{\mathrm{T}}$ is only concerned with trainees and devices, and it corresponds to a part of $\boldsymbol{Y}$, i.e. $\boldsymbol{Y}_{\mathrm{a}}=[\boldsymbol{Y}_1\quad \boldsymbol{Y}_2\quad \boldsymbol{Y}_3\quad \boldsymbol{Y}_4\quad \boldsymbol{Y}_5\quad \boldsymbol{Y}_6]$. The second is of fast varying uncertain parameters referring to, in this case, friction forces between ball screw and caps, $\boldsymbol{p}_{\mathrm{r}}=[f_{\mathrm{b}1}\quad f_{\mathrm{b}2}\quad f_{\mathrm{b}3}\quad f_{\mathrm{b}4}\quad f_{\mathrm{b}5}\quad f_{\mathrm{b}6}]^{\mathrm{T}}$. These forces vary rapidly as the position and velocity of ball screws relative to nut caps change[14], and they correspond to another part of $\boldsymbol{Y}$, i.e. $\boldsymbol{Y}_{\mathrm{r}}=[\boldsymbol{Y}_{71}\quad \boldsymbol{Y}_{72}\quad \boldsymbol{Y}_{73}\quad \boldsymbol{Y}_{74}\quad \boldsymbol{Y}_{75}\quad \boldsymbol{Y}_{76}]$. The third is $\boldsymbol{Z}=\boldsymbol{Y}_8$ exclusive of uncertain parameters. The uncertainty of this part can be considered as external disturbance $\boldsymbol{D}$. The final complete dynamic model of motion platform becomes

$$\boldsymbol{M}\ddot{\boldsymbol{X}}+\boldsymbol{H}=\boldsymbol{Y}_{\mathrm{a}}\boldsymbol{p}_{\mathrm{a}}+\boldsymbol{Y}_{\mathrm{r}}\boldsymbol{p}_{\mathrm{r}}+\boldsymbol{Z}=\boldsymbol{J}^{\mathrm{T}}\boldsymbol{F}+\boldsymbol{D}\qquad(6)$$

3 Design of Nonlinear Self-adaptive Sliding Controller

With the uncertain parameters categorized into constant and time-varying ones, the nonlinear self-adaptive control scheme can be used to estimate constant uncertain parameters[15-16] and, at the same time, the sliding control scheme is used to improve system robustness to fast varying uncertain parameters and external disturbance[15].

Given:

$$\tilde{\boldsymbol{X}}=\boldsymbol{X}-\boldsymbol{X}_{\mathrm{d}}$$

$$\dot{\boldsymbol{X}}_{\mathrm{r}}=\dot{\boldsymbol{X}}_{\mathrm{d}}-\boldsymbol{\varLambda}\tilde{\boldsymbol{X}}$$

$$\boldsymbol{s}=\dot{\boldsymbol{X}}-\dot{\boldsymbol{X}}_{\mathrm{r}}=\dot{\tilde{\boldsymbol{X}}}+\boldsymbol{\varLambda}\tilde{\boldsymbol{X}}$$

where $\boldsymbol{s}$ is the sliding surface, $\boldsymbol{X}_{\mathrm{d}}$ and $\dot{\boldsymbol{X}}_{\mathrm{d}}$ are the target position and velocity, $\boldsymbol{X}_{\mathrm{r}}$ is the virtual reference trajectory[15] used to ensure the absence of steady-state errors in final tracking trajectory and $\boldsymbol{\varLambda}$ is a constant matrix whose eigenvalues have to be strictly confined to the right half of the complex plane.

3.1 Controller design

The Controller can be expressed as follows

$$\boldsymbol{F}=\boldsymbol{F}_{\mathrm{a}}+\boldsymbol{F}_{\mathrm{s}}$$

where,

$$\boldsymbol{F}_{\mathrm{a}}=\boldsymbol{J}^{-\mathrm{T}}(\hat{\boldsymbol{M}}\ddot{\boldsymbol{X}}_{\mathrm{r}}+\hat{\boldsymbol{H}}-\boldsymbol{K}_{\mathrm{D}}\boldsymbol{s})=\boldsymbol{J}^{-\mathrm{T}}(\boldsymbol{Y}_{\mathrm{a}}\hat{\boldsymbol{p}}_{\mathrm{a}}+\boldsymbol{Y}_{\mathrm{r}}\boldsymbol{p}_{\mathrm{r}0}+\boldsymbol{Z}_0-\boldsymbol{K}_{\mathrm{D}}\boldsymbol{s})$$

refers to the control action of nonlinear self-adaptive controller, and

$$\boldsymbol{F}_{\mathrm{s}}=\boldsymbol{J}^{-\mathrm{T}}(-\boldsymbol{k}\,\mathrm{sat}(\boldsymbol{s}/\phi))$$

is the control action of sliding controller.

Thus, the final form of proposed controller appears as

$$\boldsymbol{F}=\boldsymbol{J}^{-\mathrm{T}}(\boldsymbol{Y}_{\mathrm{a}}\hat{\boldsymbol{p}}_{\mathrm{a}}+\boldsymbol{Y}_{\mathrm{r}}\boldsymbol{p}_{\mathrm{r}0}+\boldsymbol{Z}_0-\boldsymbol{K}_{\mathrm{D}}\boldsymbol{s}-\boldsymbol{k}\,\mathrm{sat}(\boldsymbol{s}/\phi))\qquad(7)$$

where $\hat{\boldsymbol{p}}_{\mathrm{a}}$ is the estimated, $\boldsymbol{p}_{\mathrm{a}}$ the value of self-adaptive controller, $\boldsymbol{p}_{\mathrm{r}0}$ the nominal value of $\boldsymbol{p}_{\mathrm{r}}$, $\boldsymbol{Z}_0$ the nominal value of $\boldsymbol{Z}$, $\boldsymbol{K}_{\mathrm{D}}$ a positive definite constant matrix, $\boldsymbol{k}\ \mathrm{sat}(\boldsymbol{s}/\phi)$ stands for the 6×1 vector of components $k_i\ \mathrm{sat}(s_i/\phi)$, $i=1,2,\cdots 6$, $\boldsymbol{k}$ the switching gain vector of a sliding controller which will be determined later, $\mathrm{sat}(\boldsymbol{s}/\phi)$ a boundary layer used to eliminate the chattering effect of sliding control and ϕ the thickness of a boundary layer.

3.2 Adaptation law of uncertain parameters

The dynamic models expressed by Nowton-Euler and Langarian separately are essentially identical[17], so

$$\boldsymbol{M}(\boldsymbol{X})\ddot{\boldsymbol{X}}+\boldsymbol{H}(\boldsymbol{X},\dot{\boldsymbol{X}})=\boldsymbol{M}(\boldsymbol{X})\ddot{\boldsymbol{X}}+\boldsymbol{C}(\boldsymbol{X},\dot{\boldsymbol{X}})\dot{\boldsymbol{X}}+\boldsymbol{G}(\boldsymbol{X})$$

Let Lyapunov function be

$$V=\frac{1}{2}\boldsymbol{s}^{\mathrm{T}}\boldsymbol{M}\boldsymbol{s}+\frac{1}{2}\tilde{\boldsymbol{p}}_{\mathrm{a}}^{\mathrm{T}}\boldsymbol{\Gamma}^{-1}\tilde{\boldsymbol{p}}_{\mathrm{a}}$$

where $\tilde{\boldsymbol{p}}_{\mathrm{a}}=\hat{\boldsymbol{p}}_{\mathrm{a}}-\boldsymbol{p}_{\mathrm{a}}$. In the same way symbols are found to be $(\tilde{\cdot})=(\hat{\cdot})-(\cdot)$ in the following.

Differentiate V, obtain

$$\dot{V}=\boldsymbol{s}^{\mathrm{T}}\boldsymbol{M}\dot{\boldsymbol{s}}+\frac{1}{2}\boldsymbol{s}^{\mathrm{T}}\dot{\boldsymbol{M}}\boldsymbol{s}+\tilde{\boldsymbol{p}}_{\mathrm{a}}^{\mathrm{T}}\boldsymbol{\Gamma}^{-1}\dot{\tilde{\boldsymbol{p}}}_{\mathrm{a}}=\boldsymbol{s}^{\mathrm{T}}(\boldsymbol{M}\ddot{\boldsymbol{X}}-\boldsymbol{M}\ddot{\boldsymbol{X}}_{\mathrm{r}})+\boldsymbol{s}^{\mathrm{T}}[\frac{1}{2}(\dot{\boldsymbol{M}}-2\boldsymbol{C})+\boldsymbol{C}]\boldsymbol{s}+\tilde{\boldsymbol{p}}_{\mathrm{a}}^{\mathrm{T}}\boldsymbol{\Gamma}^{-1}\dot{\tilde{\boldsymbol{p}}}_{\mathrm{a}}$$

Apply the property

$$\boldsymbol{y}^{\mathrm{T}}[\frac{1}{2}\dot{\boldsymbol{M}}(\boldsymbol{X})-\mathbf{C}(\boldsymbol{X},\dot{\boldsymbol{X}})]\boldsymbol{y}=0,\quad \forall\boldsymbol{y}\in\mathbf{R}^{n}$$

then

$$\dot{V}=\boldsymbol{s}^{\mathrm{T}}(\boldsymbol{JF}+\boldsymbol{D}-\boldsymbol{C}\dot{\boldsymbol{X}}-\boldsymbol{G}+\boldsymbol{C}\dot{\boldsymbol{X}}-\boldsymbol{C}\dot{\boldsymbol{X}}_{\mathrm{r}}-\boldsymbol{M}\ddot{\boldsymbol{X}}_{\mathrm{r}})+\tilde{\boldsymbol{p}}_{\mathrm{a}}^{\mathrm{T}}\boldsymbol{\Gamma}^{-1}\dot{\tilde{\boldsymbol{p}}}_{\mathrm{a}}=\boldsymbol{s}^{\mathrm{T}}[\hat{\boldsymbol{M}}\ddot{\boldsymbol{X}}_{\mathrm{r}}+\hat{\boldsymbol{C}}\dot{\boldsymbol{X}}_{\mathrm{r}}+\hat{\boldsymbol{G}}-\boldsymbol{M}\ddot{\boldsymbol{X}}_{\mathrm{r}}-\boldsymbol{C}\dot{\boldsymbol{X}}_{\mathrm{r}}-\boldsymbol{G}+\boldsymbol{D}-\boldsymbol{K}_{\mathrm{D}}\boldsymbol{s}-\boldsymbol{k}\ \mathrm{sat}(\boldsymbol{s}/\phi)]+\tilde{\boldsymbol{p}}_{\mathrm{a}}^{\mathrm{T}}\boldsymbol{\Gamma}^{-1}\dot{\tilde{\boldsymbol{p}}}_{\mathrm{a}}=\boldsymbol{s}^{\mathrm{T}}\bullet[-\boldsymbol{K}_{\mathrm{D}}\boldsymbol{s}+\boldsymbol{Y}_{\mathrm{r}}\tilde{\boldsymbol{p}}_{\mathrm{r}}+\boldsymbol{D}-\boldsymbol{k}\ \mathrm{sat}(\boldsymbol{s}/\phi)]+\tilde{\boldsymbol{p}}_{\mathrm{a}}^{\mathrm{T}}(\boldsymbol{\Gamma}^{-1}\dot{\tilde{\boldsymbol{p}}}_{\mathrm{a}}+\boldsymbol{Y}_{\mathrm{a}}^{\mathrm{T}}\boldsymbol{s})=\boldsymbol{s}^{\mathrm{T}}[\hat{\boldsymbol{M}}\ddot{\boldsymbol{X}}_{\mathrm{r}}+\hat{\boldsymbol{C}}\dot{\boldsymbol{X}}_{\mathrm{r}}+\tilde{\boldsymbol{G}}+\boldsymbol{D}-\boldsymbol{K}_{\mathrm{D}}\boldsymbol{s}-\boldsymbol{k}\ \mathrm{sat}(\boldsymbol{s}/\phi)]+\tilde{\boldsymbol{p}}_{\mathrm{a}}^{\mathrm{T}}\boldsymbol{\Gamma}^{-1}\dot{\tilde{\boldsymbol{p}}}_{\mathrm{a}}=\boldsymbol{s}^{\mathrm{T}}[\boldsymbol{Y}_{\mathrm{a}}\tilde{\boldsymbol{p}}_{\mathrm{a}}+\boldsymbol{Y}_{\mathrm{r}}\tilde{\boldsymbol{p}}_{\mathrm{r}}+\boldsymbol{D}-\boldsymbol{K}_{\mathrm{D}}\boldsymbol{s}-\boldsymbol{k}\ \mathrm{sat}(\boldsymbol{s}/\phi)]+\tilde{\boldsymbol{p}}_{\mathrm{a}}^{\mathrm{T}}\boldsymbol{\Gamma}^{-1}\dot{\tilde{\boldsymbol{p}}}_{\mathrm{a}}$$

Note

$$\boldsymbol{Y}_{\mathrm{r}}\tilde{\boldsymbol{p}}_{\mathrm{r}}+\boldsymbol{D}-\boldsymbol{k}\ \mathrm{sat}(\boldsymbol{s}/\phi)=\{\sum_{j=1}^{6}Y_{\mathrm{r}ij}\tilde{p}_{\mathrm{r}j}+D_i-k_i\mathrm{sat}(s_i/\phi)\},\ i=1,2,\cdots,6$$

choose

$$k_i=\sum_{j=1}^{6}\left|Y_{\mathrm{r}ij}\right|\bar{p}_{\mathrm{r}j}+\bar{D}_i+\varepsilon_i,\quad i=1,2,\cdots,6 \tag{8}$$

$$\dot{\tilde{\boldsymbol{p}}}_{a}=-\boldsymbol{\Gamma}\boldsymbol{Y}_{\mathrm{a}}^{\mathrm{T}}\boldsymbol{s} \tag{9}$$

where $\bar{p}_{\mathrm{r}j}\geqslant|\tilde{p}_{\mathrm{r}j}|$ is the upper limit of the estimation error of uncertain parameters, $\bar{D}_i\geqslant|D_i|$ is the upper limit of external disturbance, the positive ε_i stands for the speed approaching sliding surface and $\boldsymbol{\Gamma}$ is a symmetric positive definite matrix, which represents the learning speed of parameters.

Thus, is obtained

$$\dot{V}\leqslant-\boldsymbol{s}^{\mathrm{T}}\boldsymbol{K}_{\mathrm{D}}\boldsymbol{s}-\sum_{i=1}^{6}\varepsilon_i|s_i|\leqslant 0$$

From the above, it follows that the proposed control scheme is stable with tracking error able to be converged to zero in a finite time, and the adaptation law can be achieved as

$$\dot{\hat{\boldsymbol{p}}}_{\mathrm{a}}=-\boldsymbol{\Gamma}\boldsymbol{Y}_{\mathrm{a}}^{\mathrm{T}}\boldsymbol{s} \tag{10}$$

In order to avoid the drift of estimated parameters, the self-adaptation of parameters must stop when the system trajectories reach in the boundary layers, and at the same time, the σ-modification[18] can be included in adaptation law to further ensure the robustness of parameter adaptation.

The final parameter adaptation law takes the form of

$$\dot{\hat{\boldsymbol{p}}}_{\mathrm{a}}=-\boldsymbol{\Gamma}[\boldsymbol{Y}_{\mathrm{a}}^{\mathrm{T}}\boldsymbol{s}+\sigma(\hat{\boldsymbol{p}}_{\mathrm{a}}-\boldsymbol{p}_{\mathrm{a}0})] \tag{11}$$

where $\sigma>0$ is used to increase the robustness of the close-loop system, and $\boldsymbol{p}_{\mathrm{a}0}$ is the initial value of $\boldsymbol{p}_{\mathrm{a}}$.

Therefore, the control law Eq.(7) together with the self-adaptation law Eq.(11) yields a globally stable self-adaptive sliding controller.

4 Computer Simulation

Computer simulation is fulfilled to verify the effectiveness of the proposed control scheme. The parameters of simulation model are taken from the motion platform in the six-DOF flight simulator built in our own laboratory and their values are calculated by the aid of CAD models. The mass of the platform payload is 45.2 kg; the mass center is $(0,0,0.25)$; the inertia moment of the platform payload is $\mathrm{diag}(11.9,12.6,11.3)$, the peak torque of motor is 60 N·m and the lead of ball guide screw 0.064 m. The parameters of controller are chosen to be: $\boldsymbol{\Lambda}=10\boldsymbol{E}_6$, ϕ = 0.03, $\bar{p}_{\mathrm{r}j}=100$, $\bar{D}_i=1\ 000$, ε_i = 0.1, $\boldsymbol{K}_{\mathrm{D}}$ = 3 000$\boldsymbol{E}_6$, $\boldsymbol{\Gamma}$ = 10$\boldsymbol{E}_6$, and $\boldsymbol{E}_6$ is the 6×6 identity matrix.

4.1 Learning of the constant uncertain parameters

Since the total weight of devices and operators in a flight simulator varies to a large extent, and the moving platform is relatively lighter against the payload, an initial identification of parameters is needed to ensure a better tracking performance of platform in operation. The adaptation law is based on the tracking error which often requires a longer stretch of time to minimize owing to the relatively larger controller gain $\boldsymbol{K}_{\mathrm{D}}$. This results in a very slow adaptation process. To solve this problem, the controller gain is temporarily decreased to speed up parameter learning process in a stable close-loop system. The controller gain reverts to type as the process of initial parameter identification ends.

The reference tracking trajectory used in simulation is $[a\sin t \;\; a\sin t \;\; a\sin t \;\; b\sin t \;\; b\sin t \;\; b\sin t]$, something that possesses three translational and three rotational degrees using sine motion as reference trajectory. This reference trajectory makes all constant uncertain parameters to be simultaneously adapted. In the above-mentioned expression, $a = 0.1$, $b = 0.2$, and the period of sine motion is 1 s. External disturbance $\boldsymbol{D}$ and time-varying friction forces between ball screws and nut caps are all taken into consideration in the computer simulation.

The results from adaptation are shown in Fig.2 below.

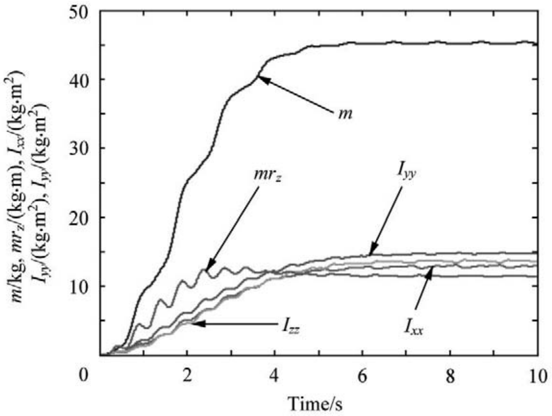

Fig.2 Parameters adaptation process.

From the Fig.2, it can be seen that all the parameters to be adapted have converged in a short time. Table 1 compares practical and adapted values of the uncertain parameters below.

Table 1 Comparison of practical and adapted values of uncertain parameters

Parameters	Practical values	Adapted values
m/kg	45.2	45.1
I_{xx}/(kg·m^2)	11.9	12.9
I_{yy}/(kg·m^2)	12.6	14.7
I_{zz}/(kg·m^2)	11.3	13.4
mr_z/(kg·m^2)	11.3	11.3

Due to the external disturbance and noise involved in the measured data by sensors, the learning speed of parameters in practice will not be such as is under the ideal conditions. However, the simulation study still demonstrates the potential of using the proposed controller to learn the parameters of a motion platform in flight simulator.

4.2 Robustness to time-varying uncertain parameters and external disturbances

In order to further evaluate the robustness of nonlinear self-adaptive sliding controller to external disturbances and uncertainties, the performances of the proposed adaptive sliding controller and the nonlinear self-adaptive controller exclusive of sliding parts with the results of the simulation are compared. In the simulation, circle motion is used as the reference trajectory. The time length of a circle motion is 10 s and the radius of the circle is 0.1 m. The simulation lasts 10 s. After 5 s, an external disturbance on the x axis is applied, with an amplitude of 500 N, enduring 5 s. The tracking performances and errors of the two control schemes are compared in Fig.3 and Fig.4. The curve Ref represents reference circle trajectory, while the curves $\boldsymbol{F}_{\mathrm{a}}+\boldsymbol{F}_{\mathrm{s}}$ and $\boldsymbol{F}_{\mathrm{a}}$ stand for adaptive sliding controller and nonlinear adaptive controller separately.

The Fig.3 and Fig.4 attest to the relatively higher tracking precision of the nonlinear adaptive sliding controller at an existence of sudden external disturbances.

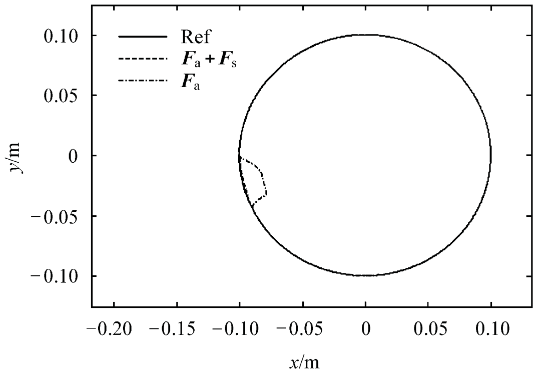

Fig.3 Circle trajectory tracking.

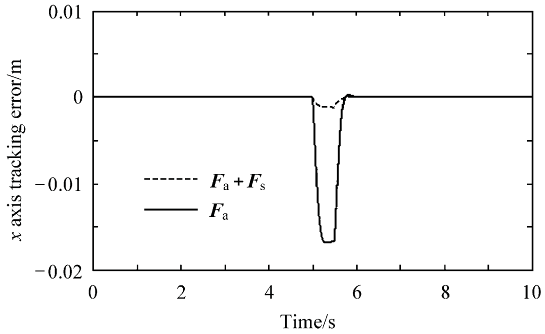

Fig.4 Circle tracking error of x axis.

5 Conclusions

A modern six-DOF flight simulator needs a motion platform having high performances. In this paper, a complete linear dynamic model of motion platform in a flight simulator has been established with the help of Newton-Euler method and, on its base, a nonlinear self-adaptive sliding controller in task space is proposed. The controller divides uncertain parameters into two groups: the constant and the time-varying. A nonlinear self-adaptive control is used to estimate the constant uncertain parameters on-line while a sliding control to compensate time-varying uncertain parameters and external disturbances. The results from simulation show that the proposed controller has ability as much to precisely identify parameters of a motion platform like loads, inertial moments, mass center etc, as to achieve precise motion control in the presence of uncertain parameters and external disturbance. Further is required verification of the performances of the control in a practical system by means of algorithm.

References

[1] Jia R Z, Peng X Y, Wang X R. Modelling and validation, performance test and evaluation for flight simulator. Acta Aeronautica et Astronautica Sinica 1998; 19(1): 41-44. [in Chinese]

[2] Rolfe J M, Staples K J. Flight simulation. London: Cambridge University Press, 1986.

[3] Stewart D. A platform with six degree-of-freedom. Proceedings of the Institute for Mechanical Engineering 1965; 180:371-386.

[4] Li Q L, Wu H T, Li L Y, et al. Kinematic analysis of the Stewart machine tool. Acta Aeronautica et Astronautica Sinica 1999; 20(2): 184-186. [in Chinese]

[5] Dasgupta B, Mruthyunjaya T S. The Stewart platform manipulator: a review. Mechanism and Machine Theory 2000; 35(1): 15-40.

[6] Lebret G, Liu K, Lewis F L. Dynamic analysis and control of a Stewart platform manipulator. Journal of Robotic System 1993; 10(5):629-655.

[7] Dasgupta B, Mruthyunjaya T S. Closed-form dynamic equations of the general Stewart platform through the Newton-Euler approach. Mechanism and Machine Theory 1998; 33(7): 993-1012.

[8] Su Y X, Duan B Y, Zheng C H. Nonlinear PID control of a six-DOF parallel manipulator. IEE Proceedings on Control Theory and Applications 2004; 151(1): 95-102.

[9] Honegger M, Brega R, Schweitzer G. Application of a nonlinear adaptive controller to a 6 DOF parallel manipulator. Proceedings of the 2000 IEEE International Conference on Robotics and Automation, IEEE, 2000; 1930-1935.

[10] Kang J Y, Kim D H, Lee K I. Robust tracking control of Stewart platform. Proceedings of the 35th Conference on Decision and Control, IEEE, 1996; 3014-3019.

[11] Ting Y, Chen Y S, Wang S M. Task-space control algorithm for Stewart platform. Proceedings of the 38th Conference on Decision and Control, IEEE, 1999; 3857-3862.

[12] Kim H S, Cho Y M, Lee K I. Robust nonlinear task space control for 6 DOF parallel manipulator. Automatica 2005; 41(9): 1591-1600.

[13] Dieudonne J E, Parrish R V, Bardusch R E. An actuator extension transformation for a motion simulator and an inverse transformation applying Newton-Raphson's method. NASA Technical Report D-7067, 1972.

[14] Huang P Y, Chen Y Y, Chen M S. Position-dependent friction compensation for ballscrew tables. Proceedings of the 1998 IEEE International Conference on Control Applications, IEEE, 1998; 863-867.

[15] Slotine J E, Li W. Applied nonlinear control. Prentice Hall, 1991.

[16] Sadegh N, Horowitz R. Stability and robustness analysis of a class of adaptive controller for robotic manipulators. International Journal of Robotics Research 1990; 9(3): 74-92.

[17] Yiu Y K, Cheng H, Xiong Z H, et al. On the dynamics of parallel manipulators. Proceedings of the 2001 IEEE International Conference on Robotics and Automation, IEEE, 2001; 3766-3771.

[18] Spooner J T, Passino K M. Stable adaptive control using fuzzy systems and neural networks. IEEE Trans on Fuzzy Systems 1996; 4: 339-359.

Biographies:

Wu Dongsu Born in 1980, he is now a doctoral student in the College of Civil Aviation, Nanjing University of Aeronautics and Astronautics. His main academic interests are nonlinear adaptive and robust control in aircraft and vehicles.

E-mail: tissle@nuaa.edu.cn

Gu Hongbin Born in 1957, a Ph.D., he is a professor in Nanjing University of Aeronautics and Astronautics. In 1997, as a senior visiting scholar, he did cooperative research in USA. His main academic interests are landing gears and aircraft, numerical simulation and control of electromechanical system.

E-mail: ghb@nuaa.edu.cn